Manuscript Details

Manuscript number	MOLLIQ_2017_4460_R1
Title	Optical and X-ray scattering studies of the electric field-induced orientational order in colloidal suspensions of pigment nanorods
Article type	Research paper

Abstract

Under pulsed or a.c. electric fields, colloidal suspensions of nanorods can show strong electro-optic effects, such as the Kerr effect, with fast response times (a few ms), which makes them good candidates for some commercial applications. For this purpose, suspensions of Pigment red 176 nanorods in dodecane were recently developed and their physical properties have been studied. We report here on the investigation of the orientational order induced by electric fields in isotropic suspensions of pigment nanorods by three different techniques: transient electric birefringence, transient electric dichroism, and in-situ small-angle X-ray scattering under electric field ("Electro-SAXS"). We show that, in spite of the apolar character of the solvent, the Maxwell-Wagner-O'Konski mechanism (i.e. the polarization of the counter-ion cloud around each particle) is responsible for the field-induced alignment of the nanorods. Although the particles are only weakly charged and the dielectric constant of dodecane is low, the pigment nanorods effectively behave as metallic particles in an insulating matrix and reach strong values (S ~ 0.5) of the induced nematic order parameter at moderate field amplitudes (~ 1 V/μm). This study confirms the feasibility of using suspensions of Pigment red 176 nanorods in dodecane for electro-optic applications.

Keywords	Transient electric birefringence; transient electric dichroism; colloids; nanorods; field-induced order.
Corresponding Author	Ivan Dozov
Corresponding Author's Institution	Laboratoire de Physique des Solides, CNRS, Université Paris-Sud
Order of Authors	Oleksandr Buluy, Natalie Aryasova, Oleksandr Tereshchenko, Yuriy Kurioz, Vassili Nazarenko, Alexey Eremin, Ralf Stannarius, Susanne Klein, Claire Goldmann, Patrick Davidson, Ivan Dozov, Yuriy Reznikov
Suggested reviewers	Eric Grelet, Alfons van Blaaderen, Angel V. Delgado, Anatoliy Glushchenko, Laurent Heux

Submission Files Included in this PDF

File Name [File Type]

Cover Letter.docx [Cover Letter]

Reply to the Reports of the Reviewers.docx [Response to Reviewers]

Highlights.docx [Highlights]

Manuscript_ReSubFinal.doc [Manuscript File]

To view all the submission files, including those not included in the PDF, click on the manuscript title on your EVISE Homepage, then click 'Download zip file'.

Dear Guest Editors,

Please, find the manuscript entitled "Optical and X-ray scattering studies of the electric field-induced orientational order in colloidal suspensions of pigment nanorods" by O. Buluy *et al*. that we wish to resubmit as a regular article to the Special Issue "Prof. Yuriy Reznikov" to be published in *Journal of Molecular Liquids*.

We have taken into account all the comments of the Reviewers in our revised manuscript. The details of the changes are given in the Reply to the Reviewers' Reports. We trust that the revised version will be suitable for publication in the Special Issue "Prof. Yuriy Reznikov".

Please, note that an additional Author, Dr. Susanne Klein, has been included in the Authors list. Indeed, after a discussion among the several groups collaborating on this project, we realized that Susanne contributed significantly to the elaboration and stabilization of the colloidal dispersion that we investigated. As this project was initiated and coordinated by Yuriy Reznikov, after his death, we were not aware of the role of Susanne. We apologize for this late correction of the Authors list.

With my best regards,

Ivan Dozov

Reply to the Reports of the Reviewers:

We are grateful to the Reviewers for their careful reading of our manuscript and for their generally positive assessments. We have taken into account most of their comments and included the required corrections in the revised text. Our detailed reply is given below, with the original comments of the Reviewers marked in italics:

Reviewer 1

By the way, the amount of x-ray scattering is so limited that I do not see that it deserves being part of the title. But this is just a matter of style.

Indeed, we presented only a part of our X-ray scattering results because they are less quantitative than those of the other techniques. However, we think that the X-ray results are important because they are direct evidence that, on the microscopic scale, the induced order is the same as that obtained from the macroscopic electro-optic experiments, and we prefer to keep the original title.

a) *On page 4 (no page numbers are provided in the text), paragraph beginning "The electric torque", and very often along the paper, the authors distinguish between MW and MWO relaxations; but in my view these are conceptually equivalent, and they only differ in the consieration in MWO of the surface conductivity of the double layer. I wonder if the authors mean alpha relaxation, that is strictly related to DL polarization. I suggest the authors to estimate where in frequency can one expect the alpha and MWO relaxations. This is conceptually important.*

We agree that several different mechanisms contribute to the electric torque, including the alpha-relaxation. This process, which is related to the formation of neutral electrolyte concentration gradients around the particle, is very important for the low-frequency dielectric relaxation and is different from the MW and MWO mechanisms. However, as our technique is not sensitive in the low-frequency domain due to the field attenuation, we can neglect this effect. We explain this in an additional text included before Fig. 10.

The difference between the MW and MWO mechanisms is the following: for the MW mechanism, only the contrast in bulk conductivity of the particle and the solvent is important, whereas, for the MWO mechanism, which is only active for charged particles, the contribution is due to the conductivity of the counter-ion cloud around the particles. Since the density of the charge carriers in the cloud is much larger than in the bulk, the amplitude and the relaxation frequency of this effect are large compared to the MW case.

b) *Paragraph 2.3: they mention frequency above 1 kHz "in the present case" and later on in the section, they mention 0.2 Hz to 1 MHz. Please clarify this.*

In our revised manuscript, we explained in more detail that although the field penetration is complete only for f > 1 kHz, the data are meaningful in a much larger frequency domain.

c) *Section 3.1 is extremely long; perhaps it would be a good idea to subdivide into subsections*

Following the suggestion of the Reviewer, we reorganized and subdivided this section in our new version.

d) The T-B model is on the basis of results interpretation. Some details of its basic equations should be given

Unfortunately, it is a difficult task to give the main results of the T-B model without a lengthy justification and explanation of the approximations. We consider that this will be even more confusing for the reader than to refer to the classical T-B paper.

e) PAge 11 (starting with "reorientational relaxation"): how can one explain that almost one second (2 Hz) is needed for rearranging ions from screening the field? Later on, on page 13 ("...long axis, mu_perp") a value of 8 ms is cited.

The time needed to build up the double layer is defined by the charge relaxation frequency, $f_{ch} \sim 20$ Hz, which is defined as the frequency at which the field is attenuated by a factor of $1/\sqrt{2}$ (see Fig. 5). This process is responsible for the gradual decrease of K_{av} at lower frequency, with practically complete screening below 0.5 Hz (see Fig. 6). The charge relaxation time, $\tau_{ch} = 1 / (2\pi f_{ch}) \approx 8$ *ms*, correspond to $1/\sqrt{2}$ attenuation of the field and not to its complete screening.

f) After Fig. 8, it is claimed that 80 s^-1 is in agreement with 39 s^-1

We explained in our revised text that the agreement is reasonable when one takes into account the approximations involved in the model.

g) Page 14 ("...dodecane, epsilon_s = 2.0....") I never found that the addiiton of 10 % particles (no matter how good conductors) increases the conductivity by three orders of magnitude

We revised the text in order to explain better that the increase of the conductivity is due to the impurities, mainly the surfactant, and not to the intrinsic conductivity of the particles.

h) Same page: Why not moving the dichroism discussion started here to the section on dichroism?

We need the results of this subsection for the discussion of the mechanisms. With the rearrangement of section 3.1 requested by both Reviewers, we think that this issue was corrected in our revised version.

i) Page 21 ("...waveform. Therefore.."): the discussion on why odd harmonics lead to larger E_sat, is not clear or evident.

We modified the last 5 lines of text before Fig. 13 to explain this point.

j) IN the SAXS data it is mentioned that the field is 960 V/micron, or 960000 V/mm. I wonder if this is even reachable in any lab. Is it 960 V/mm (as in the caption to Fig. 15)?

Actually, it was a typo error and we corrected it.

Reviewer 2

1. It is not clear how the relaxation frequency of mobile charges in the dispersion f_ch (f_ch is estimated at about 20 Hz) can be estimated from the frequency dependence of

A_av shown in Fig.5. (subsequently, this value is used to estimate the conductivity of the dispersion).

We modified the text preceding Fig. 5 in order to clarify this point. (See also our reply to the remark e) of Reviewer 1.)

2. *Estimates for the rotation diffusion constant D^r obtained from the fitting of the frequency dependence of the ratio K_av/K_osc and the relaxation constants tau_on and tau_off significantly differ (39 s^{-1} and 28 s^{-1}). What is the origin of this difference?*

This difference is due to the approximations adopted in both approaches: both the T-B and T-Y models used to treat the data consider an "ideal" dispersion of monodisperse cylindrical rods, whereas the real system that we investigate is much more complex. We revised the sentence addressing this comparison.

3. *The frequency dependence of the staturating field E_sat is estimated from the birefrengence data \Delta n_sat and K_av(f). Can this also be estimated from the dichroism measurements in the capillary geometry? (\Delta n_sat was estimated using the dicroism data).*

In principle, the frequency dependence of E^{sat} can be measured directly by dichroism measurements in the capillary. However, this measurement is less precise and more time-consuming than the birefringence technique. Therefore, we used dichroism only at low frequency (f = 500 Hz), corresponding to the smallest value of E^{sat}, and then used this result to recalibrate the easier and more precise birefringence measurements.

4. *The data for the electric field dependence of the order parameter S(E) obtained from the dicroism measurements for the capillary (Fig.9b) and planar cell geometries (Fig.12) look different. Clarifying remark would be helpful.*

In one of the figures, S was plotted versus E, whereas in the other one it was plotted versus E^2. To avoid any misunderstanding, we replotted S as a function of E^2 in both figures of our revised manuscript.

5. *More details on the meaning of the coupling coefficient \Delta A will ease the reading and make the paper more self-contained.*

We included after Eq. (2) a brief comment for this purpose.

6. *The notation "K_index" seems to be overloaded (the Kerr-like coefficients and the conductivity) and may lead to confusions.*

We changed the notation of the conductivity from K to κ.

7. *All abbreviations such as "PMT" and "RMS" should be explained.*

We explained the abbreviations at their first introduction

8. *Section title for the section 3.1 is a bit misleading as it additionally contains discussion of the discroism measurements in the capillary geometry. Perhaps, the different geometries should be explicitly separated by appropriate sectioning.*

Following the suggestions of both Reviewers, we reorganized and subdivided this section.

Highlights:

- Colloidal dispersions of Pigment Red 176 nanorods in dodecane display large electro-optic effects, like the Kerr effect.

- Transient birefringence study shows that the field induces strong alignment of the nanorods in isotropic dispersions.

- Transient electric dichroism and SAXS measurements under field confirm the transient birefringence study.

- Despite the apolar character of the solvent, the particle alignment is due to the Maxwell-Wagner-O'Konski mechanism.

- Thanks to their large response to the field and fast response time, these dispersions are well-suited for applications.

Optical and X-ray scattering studies of the electric field-induced orientational order in colloidal suspensions of pigment nanorods

Oleksandr Buluy[a], Natalie Aryasova[a], Oleksandr Tereshchenko[a], Yuriy Kurioz[a], Vassili Nazarenko[a],

Alexey Eremin[b], Ralf Stannarius[b], Susanne Klein[c], Claire Goldmann[d], Patrick Davidson[d], Ivan Dozov[d,*],

Yuriy Reznikov[a,d]

[a]*Institute of Physics, NAS of Ukraine, 03028, Kyiv, Ukraine*
[b]*Otto von Guericke University, Institute for Experimental Physics, Department for Nonlinear Phenomena, 39106 Magdeburg,Germany*
[c]*Centre for Fine Print Research, University of the West of England, Bristol BS3 2JT, UK*
[d]*Laboratoire de Physique des Solides, CNRS, Université Paris-Sud, Université Paris-Saclay, 91405 Orsay Cedex, France*

Abstract:
Under pulsed or a.c. electric fields, colloidal suspensions of nanorods can show strong electro-optic effects, such as the Kerr effect, with fast response times (a few ms), which makes them good candidates for some commercial applications. For this purpose, suspensions of Pigment red 176 nanorods in dodecane were recently developed and their physical properties have been studied. We report here on the investigation of the orientational order induced by electric fields in isotropic suspensions of pigment nanorods by three different techniques: transient electric birefringence, transient electric dichroism, and in-situ small-angle X-ray scattering under electric field ("Electro-SAXS"). We show that, in spite of the apolar character of the solvent, the Maxwell-Wagner-O'Konski mechanism (i.e. the polarization of the counter-ion cloud around each particle) is responsible for the field-induced alignment of the nanorods. Although the particles are only weakly charged and the dielectric constant of dodecane is low, the pigment nanorods effectively behave as metallic particles in an insulating matrix and reach strong values ($S \sim 0.5$) of the induced nematic order parameter at moderate field amplitudes (~ 1 V/µm). This study confirms the feasibility of using suspensions of Pigment red 176 nanorods in dodecane for electro-optic applications.

Keywords
Transient electric birefringence; transient electric dichroism; colloids; nanorods; field-induced order

1. Introduction

The electro-optic behavior of colloidal suspensions of nanorods (i.e. rod-like nanoparticles) that show liquid-crystalline phases has raised wide interest in recent years [1-12] from both fundamental and applied perspectives. Aqueous suspensions of anisometric particles are well known for their strong electro-optic response [13-19], due to a combination of two factors: the strong coupling of the particle orientation with the applied electric field **E**, and the strong optical anisotropy of the nanoparticles, which is either intrinsic or related to their anisometric shape [9, 20].

When a nematic suspension of nanorods is submitted to an electric field **E**, the main effect is the collective reorientation of the particles. The nematic director **n**, defining the average orientation of the particles, realigns either parallel or perpendicular to the field. However, the nematic order parameter, $S = < 3 \cos^2\theta - 1 >/ 2$, which is a function of the average angle of deviation of the rod axis from the director, θ, remains almost unchanged, and keeps its spontaneous value, usually $S > 0.8$. The behavior of an isotropic suspension under field is different. In this case, the particles are aligned individually by the field, which results in an induced nematic-like order, with a field-dependent order parameter $S(E)$. At weak fields, $S(E)$ varies as E^2, whereas at very strong fields, $S(E)$ saturates to its asymptotic value, either -1/2 or +1, depending on the anisotropy of the electrical properties of the particle.

The electric torque on the particle is due to its permanent dipole moment, **μ**, and to its excess polarizability, **α**, as compared with the same volume of solvent. Usually, in aqueous solvent, **α** is orders of magnitude larger than the intrinsic polarizability of the particle. Indeed, the high dielectric constant and the strong dissociating power of water strongly enhance the three main mechanisms of orientation of the particles under field: the dielectric mechanism, where the induced dipole is due to the accumulation of bound (polarization) charges on the particle/solvent interface [21]; the Maxwell-Wagner (MW) mechanism, with induced dipole due to the accumulation of free (conductivity) charges on the interface [22, 23]; and the Maxwell-Wagner-O'Konski (MWO) mechanism, for which the induced dipole is due to the polarization of the ionic cloud surrounding a charged particle [24, 25].

Despite the advantage of high electro-optic efficiency, aqueous colloidal suspensions are not suitable for applications. Indeed, due to their high conductivity, they suffer from fast electrochemical degradation, Joule heating, thermally- and electrophoretically-induced flow and instabilities, as well as increased energy consumption of the devices. To avoid these issues, the electro-optics of colloidal suspensions in polar and apolar organic solvents has been intensively studied in the recent years [1, 4-9]. In particular, the possibility of using colloidal suspensions for display devices has been confirmed for dispersions of different types of pigment nanorods in dodecane at high concentrations (> 15 wt% to reach the nematic phase) [26-28]. For example,

experiments performed with Pigment Red 176 nanorods, submitted to d.c. and low-frequency a.c. electric fields, showed a clear electro-optic response [26, 28, 29]. Moreover, unexpectedly, this response was affected by exposure to UV-light [26]. These experiments strongly suggested that the pigment nanoparticles bear a permanent electric dipole moment and that ionic impurities may play a role in the electro-optic response, in spite of the apolar character of the solvent.

Here we report an experimental investigation of the electric-field-induced birefringence in isotropic colloidal suspensions of pigment nanorods in an apolar solvent. The field is applied either as bursts of sinusoidal a.c. voltage with variable frequency ranging from 0.2 *Hz* up to 1 *MHz*, or as short d.c. pulses. Our results show that, despite the apolar solvent, the alignment of the particles is due mainly to the MWO mechanism, i.e. to the polarization of the counter-ion clouds around them. We also compare the results obtained with this technique with those of electric-field-induced dichroism, measured in two different experimental geometries, and with the field-induced order parameter measured by X-ray scattering.

2. Experimental

2.1.Materials

The particles of Pigment Red 176 (Novoperm Carmine HF3C from Clariant, Frankfurt am Main, Germany) used in this study (Fig. 1), are elongated platelets which can be approximated as nanorods with average dimensions of 250 ± 50 *nm* in length (*L*) and 50 ± 20 *nm* in diameter (*D*). Stable suspension with nanorod concentrations between 20 to 25wt% of solids (the so called mill base) were achieved by milling. 40wt% of the dispersant Solsperse 11200 were dissolved in dodecane, the pigment was then added and the mixture milled in a planetary mill at 500 rpm for 60 min using 0.3 mm Yttria-stabilized Zirconia beads. Suspensions with solid phase concentration of 10wt% were prepared by diluting the mill base with dodecane. The suspensions were kept for stabilization for about 24 hours in the dark. Oxygen was removed by bubbling nitrogen through the suspensions. When needed, this suspension batch was further diluted with more dodecane. All the dispersions investigated here were in the isotropic phase in absence of applied field. Moreover, the samples showed no aggregation over long times and the dispersions remained stable for years.
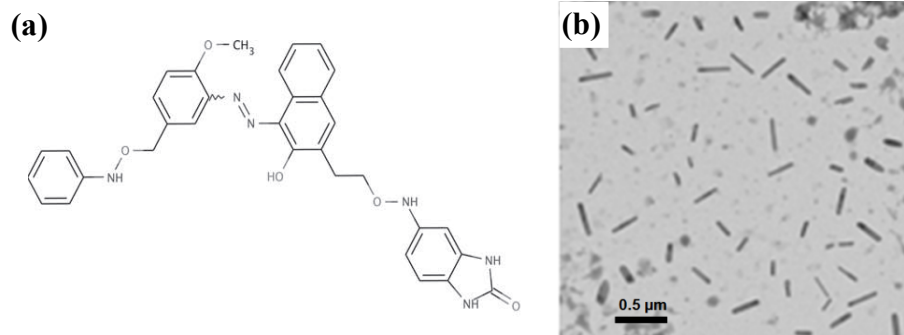
(a)

(b)

Fig. 1: (a) Chemical formula of Pigment Red 176; (b) TEM image of the pigment particles.

2.2. Transmission Electron Microscopy (TEM)

TEM observations were performed on a JEOL1400 microscope operating at 80 kV. The particles suspended in dodecane were deposited on a carbon-coated copper grid lying on an absorbent paper and dried in air.

2.3. Induced-birefringence technique

The experimental setup for the investigation of the electric-field-induced birefringence of the pigment particle dispersions has been described in detail in a previous publication [30]: The colloidal dispersion (volume fraction ϕ = 5%) was contained in a flame-sealed 100 μm optical flat glass capillary. The electric field was applied along the capillary axis by a pair of external electrodes, placed directly (2 mm apart) on the outer surface of the capillary walls. Numerical simulations of the penetration of the field show that it is quite uniform inside the colloidal dispersion when the frequency is high enough (f > 1 kHz in the present case) and that the screening losses are negligible. At lower frequencies, however, the field in the sample is attenuated because of the build-up of electric double layer on the inner surface of the capillary walls. This partial screening of the field at low frequencies is due to our external-electrodes setup. For the experimental data processing, the field screening is taken into account by using the frequency-dependence of the transient birefringence [30].

The field-induced birefringence was measured in real time, using a photomultiplier tube (PMT) detector mounted on a polarizing microscope Leitz Ortholux II, with the apparatus described in reference [30] (but using a Sénarmont compensator instead of a Berek compensator). The time-resolution was better than 1 μs and, thanks to the accumulation of a high number of transient signals (up to 64000), the phase shift resolution was less than 0.1 nm. The field was applied either as bursts of sinusoidal a.c. voltage (from 1 to 10000 periods in one burst) with variable frequency f, ranging from 0.2 Hz up to 1 MHz, or as short d.c. pulses (duration τ_p from 0.1 to 10 ms) with amplitude up to 400 V.

2.4. Induced-dichroism technique

The main dichroism experiment used a flat sandwich-type cell with the colloidal dispersion contained between glass substrates with deposited Indium-Tin Oxide (ITO) electrodes. The ITO-coated, $25 \times 25 \times 1$ mm, glass substrates were washed in an ultrasonic bath with Alconox detergent (Sigma-Aldrich) for 10 minutes at 60 ^0C and then dried. After one hour baking at 180 ^0C, the cells were assembled using identical substrates with spacing controlled by glass spheres of 20 μm in diameter (Fig. 2). To improve homogeneity of the distribution of the colloidal particles in the bulk, the suspension was sonicated before use. Filling of the cell was achieved by the pressure gradient from a vacuum pump connected to one of the open sides of the cell through rubber pipes. Filled

cells were sealed using two-component epoxy glue (DoneDeal Adhesives Lab., Inc.). Examination of the cells by optical microscopy revealed a uniform distribution of the pigment particles throughout the cells.

The light transmission through the flat cell was measured at different frequencies and amplitudes of the applied electric field. The experimental setup and geometry of the experiment are presented on Fig 2(c) and were published in detail elsewhere [31]. The setup consists of He-Ne laser, polarizer (P), cell, photodiode (PD), and input-output board (National Instruments, NI PCI-6221, and Pintek High-frequency amplifier, HA-405) driven by computer. The sampling frequency of the input-output board is 800 *kHz*, providing a resolution of 800 000 measurements per second. A square-waveform a.c. field was applied to the cell in bursts with duration of 500 *ms*. The frequency *f* and amplitude of the a.c. field were respectively varied from 1 to 100 *kHz* and from 1 to 5 *V/μm* with increments of 0.5 *V/μm*.
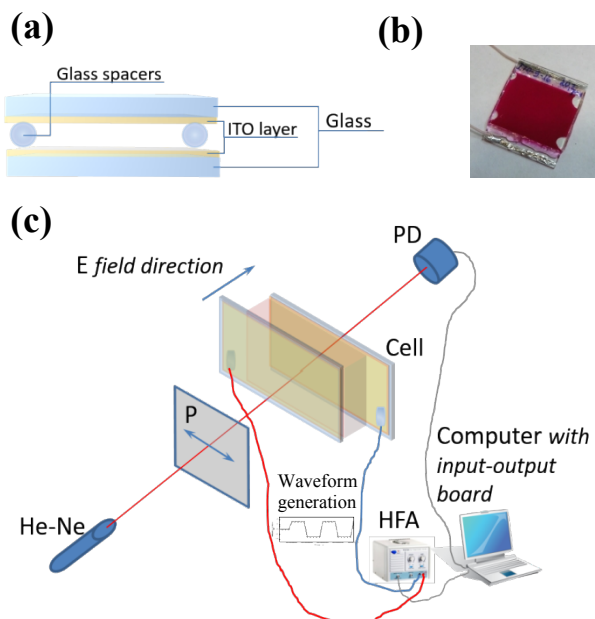

Fig. 2: Sample and set-up used in the dichroism experiment: (a) Cross-section of the cell; (b) Photograph of the 20 *μm* thick cell; (c) Sketch of the experimental setup.

2.5. *In-situ* SAXS measurements

We also studied the electric-field-induced reorientation of the pigment nanoparticles by small-angle X-ray scattering (SAXS) at the ID02 beamline of the European Synchrotron Radiation Facility (ESRF) in Grenoble, France. The beamline was already described in great detail in reference [32]. The sample of nanoparticle suspension was held in a 1 *mm* diameter cylindrical Lindemann glass capillary and the electric field was applied in-situ with the same setup used for optical measurements under the microscope and described in detail elsewhere [33]. The field amplitude was varied between 0 and 960 *V/μm* and the frequency was 2 *kHz*. The X-ray

wavelength, λ, was set to 0.0993 nm and the sample to detection distance was 2.01 m, which leads to a q-range of 0.1 – 1.5 nm^{-1}, where q is the scattering vector modulus ($q = 4\pi \sin\theta / \lambda$, with 2θ the scattering angle). A Frelon camera, with 24 μm pixel size, was used for detection and the exposure times were typically around 1 s.

3. Experimental Results and Discussion

3.1. Field-induced birefringence and dichroism in capillary cell

In the capillary cell, the field is applied perpendicularly to the direction of optical observation, which is the optimal geometry for the study of the transient birefringence and dichroism. Comparing the results of these two optical techniques, applied to the same sample, facilitate the interpretation of the data.

3.1.1. Field-induced birefringence: Experimental results

A few typical results of the birefringence measurements are shown in Figs. 3 and 4. The two sets of data, from the sinus bursts and from the d.c. pulses, give information about the excess polarizability anisotropy $\Delta\alpha$, the dipole moment $\boldsymbol{\mu}$, and the rotational diffusion constant D^r of the pigment particles. The signal measured on the PMT cathode, $A(t)$, is proportional to the transient birefringence $\Delta n(t)$. At long term, after relaxation to a steady-state regime, it can be described [34] as a sum of two contributions:

$$A(t) = A_{av}(f) + A_{osc}(f)\cos(2\omega t - \delta(f)) \ .$$

Here, $\omega = 2\pi f$ is the angular frequency of the applied field, $A_{av}(f)$ is the average (time-independent) component, $A_{osc}(f)$ is the amplitude of the component oscillating at twice the frequency of the applied field, and $\delta(f)$ is the phase shift with respect to the field. In the treatment of the sinusoidal field results, we will follow the detailed analysis [34] proposed by Thurston and Bowling (T-B), adapting it to our specific experimental conditions, i.e. the use of external electrodes.

Fig. 5 shows the frequency dependence of the average amplitude, A_{av} (f), measured for a constant voltage with root mean square (RMS) value U_{RMS}, applied to the external electrodes, and renormalized with the maximum value reached at $f_{max} = 0.5$ kHz. To understand the A_{av} (f) dependence, we need to take into account [30] that the field actually applied to the particles within the dispersion, E_{in} (f), is not the external field, E_{RMS}, because of the frequency-dependent screening losses $C_s(f) = E_{in}(f) / E_{RMS}$. The actual response of the particles at constant internal field is then $A_{av,in}$ $(f) = A_{av}$ $(f) / C_s^2(f)$. For $f >> f_{ch}$, the screening losses are negligibly small and $C_s(f) \approx 1$ (here, f_{ch} = $\kappa_s / (2\pi\varepsilon_0\varepsilon_s)$ is the relaxation frequency of the mobile charges in the dispersion, and κ_s and ε_s are respectively the conductivity and the dielectric constant of the solvent). This behavior is observed on the right-hand part of the curve on Fig. 5, where $A_{av,in}$ $(f) \approx A_{av}$ (f). On the contrary, for $f << f_{ch}$, the field is completely screened by the

charges accumulated in the suspension, in front of the electrodes and $C_s(f) \approx 0$. This behavior is clearly seen on the left-hand part of the curve in Fig. 5, for $f < f_{max}$. Approximating the charge relaxation [30] as a simple Debye relaxation, we find that f_{ch} is approximately 20 Hz from the condition $C_s(f_{ch}) = 1/\sqrt{2}$. So, for $f > f_{max} >> f_{ch}$, the screening can be neglected and $A_{av,in}\ (f) = A_{av}\ (f)$. In other words, despite the external electrodes, the signal measured in the high-frequency domain is the same as it would be with ideal (non-polarized) electrodes immersed in the liquid.
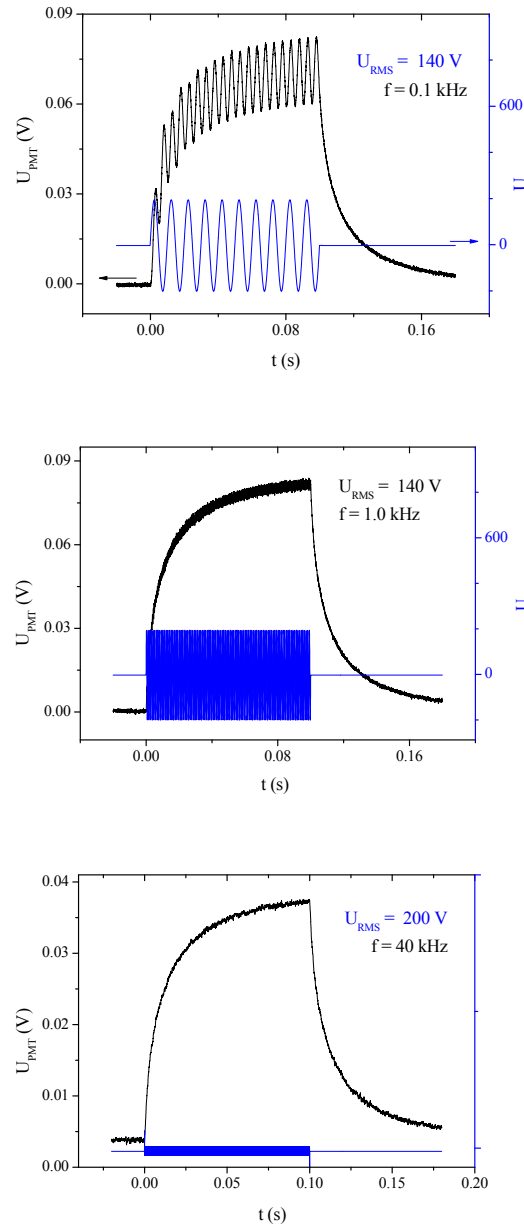
Fig. 3: Typical response to sinusoidal bursts (the applied voltage is plotted in blue) for three different frequencies. The PMT signal is proportional to the induced birefringence and it is a superposition of an average component

with amplitude A_{av} and a signal oscillating at the double frequency $2f$ (with amplitude A_{osc}). At high frequency, $f \gg 1\ kHz$, the oscillating signal is completely relaxed.
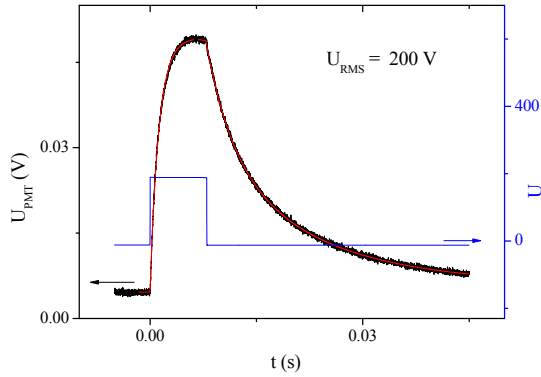

Fig. 4: Typical response to a short pulse of d.c. voltage. The two-exponential fit giving the amplitudes and the relaxation times of the on- and off- response to the field is shown in red.
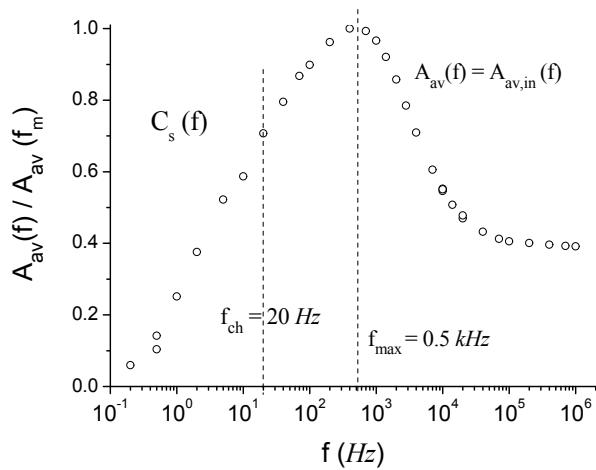

Fig. 5: Frequency dependence of the average amplitude of the induced birefringence. The decrease of the amplitude in the region $f < f_{max}$ is due to the screening of the internal field by the mobile charges. The relaxation of A_{av} (f) in the region $f > f_{max}$ is related to the MW and/or MWO mechanisms of the particle reorientation under field.

More information about the different relaxation processes can be obtained from the frequency dependences of the average and oscillating Kerr coefficients (Fig. 6), defined respectively as $K_{av} = \lim_{E \to 0} \Delta n_{av}\ (E)\ /E^2$ and $K_{osc} = \lim_{E \to 0} \Delta n_{osc}\ (E)\ /E^2$. The inspection of Fig. 6(a) reveals the presence of several relaxation processes, with characteristic frequencies of a few Hz (the relaxation of the solvent charges), of a few tens to hundreds of Hz (the orientational relaxation) and of about $5\ kHz$, whose origin is related to the relaxation mechanisms and will be discussed below. At very low frequencies, $f < 2\ Hz$, the two coefficients are approximately equal, $K_{av} \approx K_{osc}$, as expected from the T-B model for $f \ll D^r$. In this frequency domain, the observed relaxation is only due to the

screening of the field in the sample by the conductive charges of the solvent. This process influences in the same way the two Kerr coefficients, leaving their ratio, $R_K = K_{av} / K_{osc}$, unchanged.
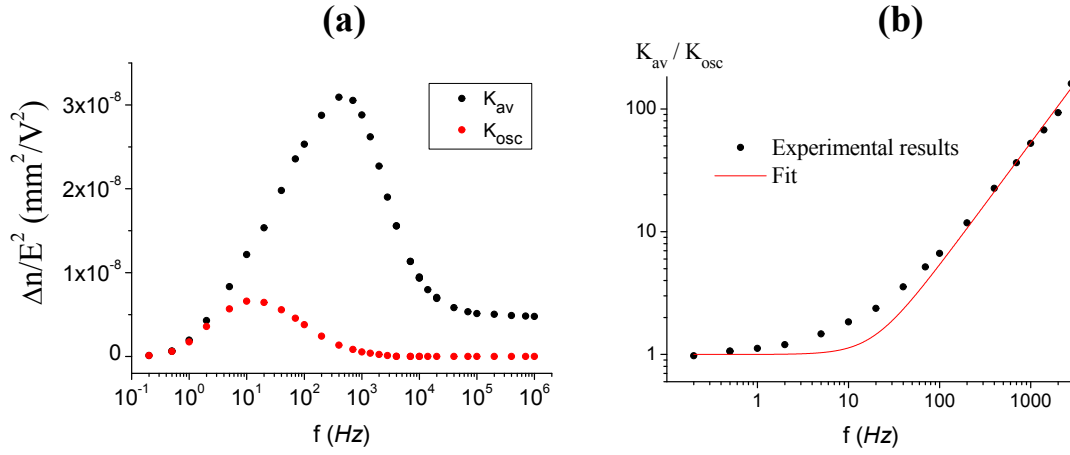

Fig. 6: Frequency dependence of the Kerr coefficients for the average and oscillating transient birefringence (a) and their ratio (b).

Above $f = 2\ Hz$, R_K increases, revealing that the orientational relaxation takes place, damping as usual the two Kerr coefficients in a distinct way. This relaxation of K_{av} and K_{osc} is related to the relaxation times for reorientation of the excess polarizability tensor $\boldsymbol{\alpha}$, $t_\alpha = 1\ /\ (6D^r)$, and the permanent dipole $\boldsymbol{\mu}$, $t_\mu = 1\ /\ (2D^r)$, of the particle. Therefore, the relaxation times of K_{av} and K_{osc} are comparable to t_α and t_μ. At low frequency, $2\pi f\, t_\mu << 1$, the two Kerr coefficients are equal, $K_{av,0} = K_{osc,0}$; at very high frequencies, $2\pi f\, t_\alpha >> 1$, the coefficients relax to $K_{osc,\infty} = 0$ and $K_{av,\,\infty} = $ const, and the ratio $K_{av,0}\ /\ K_{av,\,\infty}$ allows one to determine the relative strength of the dipolar and polarizability couplings with the field, $P = kT\Delta\alpha/\mu^2$. However, up to $f = f_{max} \approx 0.5\ kHz$, K_{av} increases with the frequency, showing that the charge relaxation still takes place in this frequency domain.

Above f_{max}, the average Kerr coefficient starts to decrease. This is only partially due to the tail of the rotational relaxation process. Indeed, at these frequencies the oscillations of the experimental curves are practically completely damped (see Fig. 3), showing that the rotational relaxation has already taken place for both Kerr coefficients, K_{av} and K_{osc}. Therefore, the decrease of K_{av} in the frequency domain $1 - 10\ kHz$ is mainly due to an additional higher-frequency relaxation process, which is not related to the rotational diffusion of the particles. This decrease can be attributed to the relaxation of the MW and/or MWO contributions to the excess polarizability (as the dielectric contribution is expected to relax at much higher frequencies). Finally, above $f = 10\ kHz$, K_{av} saturates to a high-frequency plateau, at a level about 6 times lower than the maximal value reached at $0.5\ kHz$.

Due to the additional relaxation processes, the direct analysis of the frequency dependences of K_{av} and K_{osc} using the T-B approach is impossible in our case. Moreover, the phase shift cannot either be used in the analysis

because it is also seriously affected by the unknown contributions of the additional relaxation processes . Therefore, to interpret the experimental results, we only consider the ratio K_{av} / K_{osc} (see Fig. 6b) and we fit it with the Thurston - Bowling expressions [34]. The best fit gives $P = \infty$, i.e. $\mu = 0$, and $D^r = 39 \ s^{-1}$. The experimental curve is much smoother than the theoretical one, revealing a large polydispersity of the size of the particles (and therefore of their rotational diffusion constant, D^r). We note that the absence of a permanent dipole moment derived from the T-B fit of our data contradicts the previously reported result $\mu_\perp \neq 0$ for the Pigment Red 176 [26]. However, in both studies the permanent dipole value is obtained from the measurements at very low frequencies, below the charge relaxation frequency, where the results can be seriously altered by electrophoresis and other artifacts.

When a high-frequency sinusoidal burst is applied, the amplitude of the oscillating response is zero, i.e. the particles behave as under a square pulse with field amplitude E_{RMS}. Moreover, the contribution of the permanent dipole of the particle to the reorientation torque is averaged to zero and, at least for a monodisperse system, the on- and off- relaxations of the transient birefringence are exponential, with relaxation time $\tau_{on} = \tau_{off} = 1 / (6D^r)$. Although the experimental curves (Fig.7a) are not exactly exponential because of the polydispersity, the two relaxation times are indeed almost equal, giving $D^r = 28 \ s^{-1}$. Taking into account the approximations used in the data interpretation, this is in fair agreement with the value $D^r = 39 \ s^{-1}$ deduced from the frequency dependence of the K_{av} / K_{osc} ratio. The frequency dependence of the relaxation times is almost constant (Fig. 7b). Indeed, this behavior is expected because, at high frequencies, only the polarizability anisotropy $\Delta\alpha$ contributes to the coupling with the field and the two relaxation times are equal to $t_\alpha = 1 / (6D^r)$.
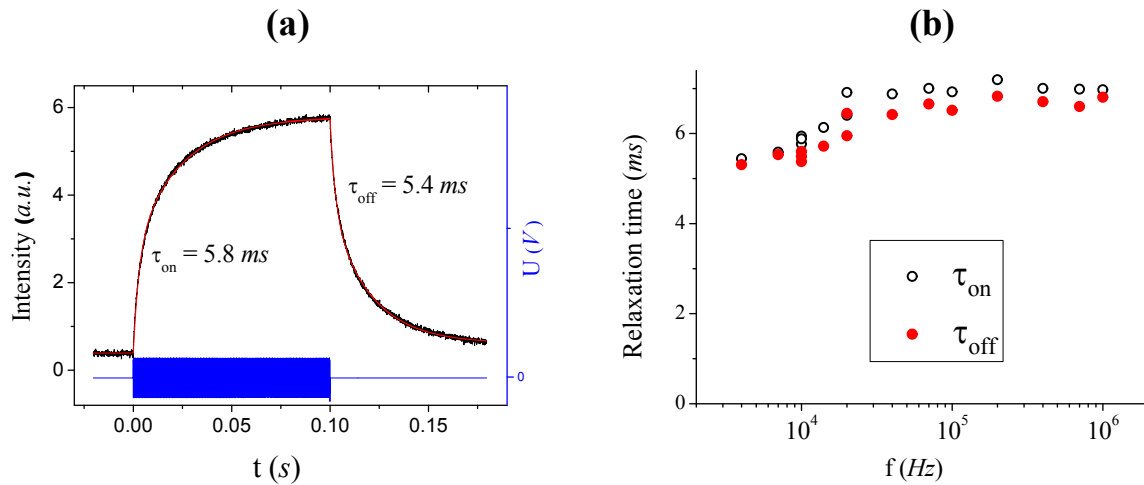
(a)　　　　　　　　　　　　　　　　　　　　**(b)**

Fig. 7: Transient birefringence induced by high-frequency sinus bursts. (a) Time dependence of the induced birefringence at $f = 10 \ kHz$. The on- and off- relaxation times are obtained from the initial slope of the two-exponential fits shown in red. (b) Frequency dependence of the relaxation times. For $f > 40 \ kHz$, where the polarizability anisotropy $\Delta\alpha$ is frequency-independent, the relaxation times remain constant, as expected.

The behavior of the transient birefringence changes when square d.c. pulses are applied (see Fig. 8). First of all, the on- and off- response times are no longer equal. The relaxation time after switching off the field, τ_{off}, is larger and it increases with increasing pulse duration, τ_p. For pulses long enough to saturate the birefringence, $\tau_p >$ 5 ms, τ_{off} reaches about 6 - 8 ms, which is comparable to the value of 7 ms obtained with long a.c. pulses. The dependence of τ_{off} on the pulse duration is the signature of the polydispersity of the particles: for short pulses, only the smallest particles contribute to the transient birefringence, resulting in faster relaxation when the field is switched off; with longer pulses, the contribution of the slowly reorienting large particles increases, and τ_{off} increases because of their smaller rotational diffusion constant. In contrast to τ_{off}, the relaxation time τ_{on} remains constant (Fig. 8(b)) and is much smaller, about 1 ms, than for the case of a.c. pulses. The case of the transient birefringence induced by d.c. pulses has been treated in detail [35] by Tinoco and Yamaoka (T-Y). From the T-Y formulae, the above behavior with $\tau_{off} > \tau_{on}$ shows that the particle has a permanent dipole perpendicular to its long axis, $\mathbf{\mu}_\perp$. However, this is in contradiction with the results from the a.c. bursts, which clearly show that the pigment particles have no permanent dipoles. Most probably, the observed behavior is influenced in our case by two phenomena which are not taken into account by the Tinoco-Yamaoka model. Indeed, we use external electrodes and, at times comparable to the relaxation time of the charges in the solvent, $\tau_{ch}= 1 / (2\pi f_{ch}) \approx 8$ ms, the external field does not penetrate efficiently in the solvent, i.e. the low-frequency components of the field acting on the particles are "filtered". In addition, under long d.c. pulses the mobile charges of the solvent are transported and accumulated on the inner faces of the glass walls of the capillary, in front of the electrodes, attenuating the field applied to the dispersion. When the field is switched off, the accumulated charges apply a field on the sample, which results in a spurious birefringence signal because the particles are still submitted to an electric field. This spurious signal then relaxes on a time scale comparable to the relaxation time of the charges, τ_{ch}. Moreover, for frequencies higher than a few kHz, the torque applied by the field on the particles varies, due to the observed additional relaxation of the polarizability that is not related to the reorientation process and therefore not taken into account in the T-Y model.

Some of the measured quantities can easily be compared to the predictions of models. Indeed, following the well-known Perrin's approach [36, 37] and approximating the pigment particles as spheroids rotating in a solvent with viscosity η_s = 1.34 $mPa.s$, we obtain D^r = 80 s^{-1} for the tumbling motion of the particles. Although this value is twice larger than the experimental one, D^r = 39 s^{-1}, the agreement is reasonable when taking into account the approximations made: the particles are not of spheroidal shape or monodisperse in size and, due to the relatively high volume fraction, ϕ = 5 %, their motions are hydrodynamically coupled, resulting in an effective viscosity higher than η_s. The charge relaxation frequency, f_{ch} = 20 Hz, is another measured value that is easy to understand. From the dielectric constant of dodecane, ε_s = 2.0, we obtain κ_s = 2.2 $\times$ 10^{-9} S/m for the conductivity of the

colloidal dispersion. This value is 2 – 3 orders of magnitude larger than the conductivity of pure dodecane [38], 7 × 10⁻¹² *S/m*. This huge increase of the conductivity is due to the (relatively) large concentration of ionic impurities coming from the nanoparticles themselves, from the dispersant used to promote the colloidal stability and (to a lesser extent) from species adsorbed on the inner surface of the capillary. To check this conductivity value, we measured the imaginary part of the dielectric constant of the pigment particle suspensions at frequency 1 *Hz* in flat cells with ITO electrodes. For pure dodecane, we obtained κ_s = 8 × 10⁻¹² *S/m*, in good agreement with the literature. With increasing pigment concentration from 1 to 10 %, the conductivity varied in the range 0.4 – 2.8 × 10⁻⁸ *S/m*. Although larger than the values derived from the capillary experiment, these values are reasonable when taking into account that, in the flat cell, additional ionic impurities are released from the ITO electrodes and the cell seal.
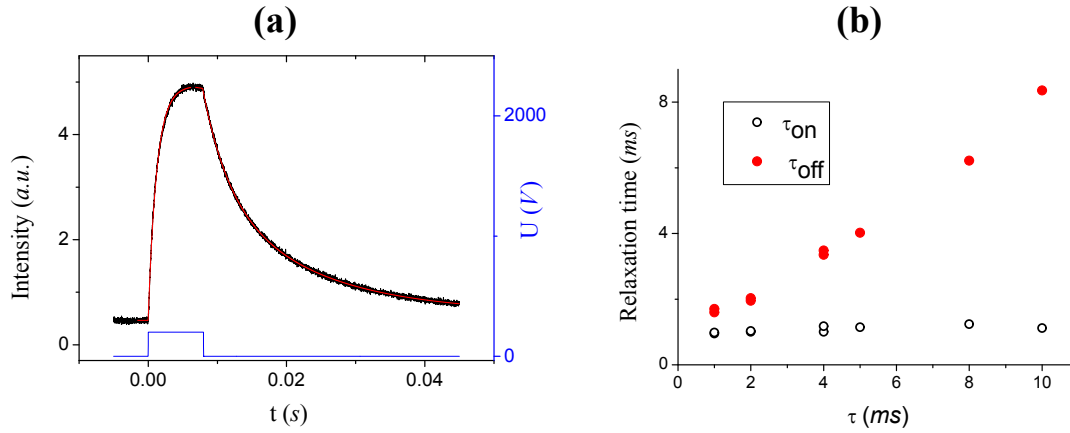

Fig. 8: Transient birefringence induced by d.c. square pulses. (a) Time dependence of the induced birefringence at E = 200 *V / mm* and pulse duration τ = 8 *ms*. The two-exponential fit is shown in red. (b) Pulse duration dependence of the on- and off- relaxation times obtained from the initial slope of the two-exponential fits of the transient birefringence.

Usually, more quantitative information about the induced orientational order parameter $S (E)$ can be obtained from the field-dependence of the average birefringence measured at fixed frequency (to simplify the notations, we omit below the subscript of Δn_{av}). Indeed, at strong enough fields, $E >> E^{sat}$, the induced order saturates to $S (E)$ = 1, which is the theoretical limit at high field, and the transient birefringence saturates to its maximum value, defined as $\Delta n^{sat} = \Delta n (E) / S (E)$ and related also to the specific birefringence of the particles, Δn^{sp}, by the expression $\Delta n^{sp} = \Delta n^{sat} / \phi$. Here the saturation field is defined as $E^{sat} = (\Delta n^{sat} / K_{av})^{1/2}$ and it gives direct information about the excess polarizability of the particles [30]. However, this approach is difficult to apply to our birefringence experiment because of the strong dichroism of the pigment particles. Indeed, at strong fields, the small birefringence signal is masked by the much stronger dichroic signal. Moreover, the light propagation and interference in the dichroic case is much more complex and difficult to analyze, resulting to prohibitively large error bars for the birefringence results. Nevertheless, both the transient birefringence and the transient dichroism

arise from the same physical mechanism, i.e. the field-induced orientational order of the particles. Therefore, we obtained the values of E^{sat} and Δn^{sat} in a separate experiment (using exactly the same geometry with external electrodes) from the transient dichroism results measured as a function of the applied field.

3.1.2. Field-induced dichroism: Experimental results

Dichroism measurements are a well-known technique used to study the orientational order in liquid crystals [39, 40]. For molecular anisotropic liquids, the dichroic ratio is a function of the order parameter S, describing the orientational order of the long molecular axis **L**, and of the angle between **L** and the absorption dipole moment **m**. This simple approach cannot be applied in our case because the complex pigment molecule has multiple chromophores and their overlapping absorption bands can be polarized in different directions. The polarization ratio of the absorbing pigment particles is also decreased by the strong interactions between the molecules, which modifies the degree of polarization of the absorption band. Moreover, like the birefringence case, the form dichroism [41] also contributes to the absorption of the nanorods. For this reason, we will describe the absorption by a more general tensorial quantity, instead of the dyadic **mm**. In a uniaxially-aligned medium, the most general form of the absorbance is a symmetric second-rank tensor **a**, with main values defined by $a_i = \log (I_0 / I_i)$, where I_0 and I_i are respectively the intensities of the incident and the transmitted light and $i = \parallel , \perp$ shows the polarization of the light with respect to the applied field. The dichroic ratio is defined as

$$R = \frac{a_\parallel - a_\perp}{a_\parallel + 2a_\perp} = \frac{\Delta a}{3a_{iso}} \ ,$$

where $\Delta a = a_\parallel - a_\perp$ is the anisotropy of the absorbance and $a_{iso} = Tr(\mathbf{a})/3$ is its isotropic part. The absorbance is proportional to the volume fraction ϕ of the particles and to the optical path length d, $\mathbf{a} = \phi d\, \mathbf{k}$, where **k** is the extinction coefficient (absorbance per unit length) extrapolated to $\phi = 1$. As **k** is actually a uniaxial second rank tensor, its anisotropy Δk is proportional to the induced order parameter, $\Delta k = S(E)\, \Delta k^{sat}$, where Δk^{sat} is the saturated value of the extinction anisotropy, reached under extremely strong field. However, the isotropic part of **k**, $k_{iso} = Tr(\mathbf{k})/3$, is field-independent. For the field-variation of the dichroic ratio, we then obtain an expression similar to that used to analyze the field dependence of Δn:

$$R(E) = \frac{k^{sat}_\parallel - k^{sat}_\perp}{k^{sat}_\parallel + 2k^{sat}_\perp} S(E) = R^{sat} S(E), \tag{1}$$

where $R^{sat} = R(E = \infty)$.

The main dichroic results, measured at $f = 500\ Hz$, are presented in Fig. 9. The dichroic ratio is positive, which indicates that the extinction coefficient is larger for light polarized along the nanorod axis (as expected for form dichroism). By extrapolating the results for $E \rightarrow \infty$, we obtain the saturated value of the dichroic ratio, $R^{sat} =$

0.31, the dichroic analog of the Kerr coefficient, $C_R = lim_{E \to 0} R(E) / E^2 = 7.4 \times 10^{-7}$ mm^2/V^2, the saturating field, $E^{sat} = (R^{sat} / C_R)^{1/2} = 650$ V/mm, and the field-dependence of the order parameter (see Fig. 9b), $S(E) = R(E) / R^{sat}$.
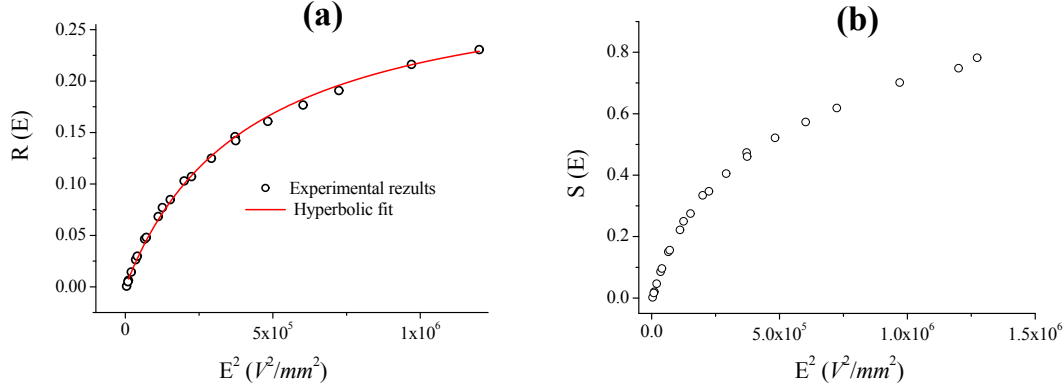

(a)

(b)

Fig. 9: Plot of the induced dichroic ratio $R(E)$ versus E^2 **(a)** and the induced nematic order parameter $S(E)$ **(b)**. The transient dichroism is measured under bursts of sinusoidal voltage ($f = 500$ Hz).

3.1.3. Discussion of the mechanism of the field-induced reorientation of the pigment particles

Comparing these dichroic results with the birefringence data at $f = 500$ Hz, $E_{RMS} = 140$ V, we obtain $\Delta n^{sat} = 0.0132$ and $\Delta n^{sp} = 0.264$. The specific birefringence Δn^{sp} can be approximately decomposed in two parts: the intrinsic birefringence of the bulk material, Δn^{intr}, and the form birefringence, Δn^{form}, which depends on the particle aspect ratio and the particle/solvent contrast of refractive indices [20, 42]. The absence of literature data for the pigment indices $n^p_{\parallel}$ and $n^p_{\perp}$ complicates the quantitative analysis of these two contributions. Qualitatively, the large measured value of the specific birefringence suggests that both these contributions are large, i.e. that $n^p_{\parallel}$ and $n^p_{\perp}$ are large compared to the solvent index $n_s = 1.42$ and/or the intrinsic birefringence of the pigment $\Delta n^{intr} = n^p_{\parallel} - n^p_{\perp}$ is quite high. These large values of the refractive indices of the pigment seem realistic when taking into account that we measure the birefringence at $\lambda = 546$ nm, i.e. in the high-dispersion region of n^p due to the strong and highly anisotropic absorption band of the pigment for blue light.

The saturating field, E^{sat}, can be calculated as a function of the frequency f from the measured values of Δn^{sat}, which is frequency-independent, and from the Kerr coefficient $K_{av}(f)$. With increasing frequency, E^{sat} increases from its minimum value at 500 Hz, $E^{sat} = 650$ V/mm, up to $E^{sat} = 1660$ V/mm at 1 MHz on the high-frequency plateau of $K_{av}(f)$. These values give an important information about the anisotropy of the excess polarizability of the particle $\Delta \alpha$ and, therefore, about the mechanism of particle orientation in the electric field. For rod-like particles, the coefficient ΔA, which describes the coupling with the electric field, is simply [30]

$$\Delta A = \frac{\Delta \alpha}{kT} = \frac{15}{\left(E^{sat}\right)^2} ,$$

(2)

resulting in $\varDelta A = 3.5 \times 10^{-11}$ m^2/V^2 at $f = 500$ Hz and $\varDelta A = 5.4 \times 10^{-12}$ m^2/V^2 at $f = 1$ MHz (Fig. 10). We note that the coupling parameter $\varDelta A$, which is the anisotropy of the excess polarizability of the particle in kT-units, carries all the information about the energy of the induced dipole of the particle under field.

Three main mechanisms contribute to $\varDelta A$. The first one is related to the polarization of the bound charges at the particle surface. This purely dielectric contribution, $\varDelta A_{diel}$, depends only on the aspect ratio of the particle and the respective dielectric constants [13]. Moreover, the relaxation frequency of $\varDelta A_{diel}$ is very high, in the optical frequency range, far beyond the frequencies explored here. The second mechanism, the Maxwel-Wagner (MW) polarization is related to the accumulation on the particle surface of mobile (conductivity) charges, which takes place when at least one of the media is an imperfect dielectric, with finite conductivity [22, 23]. Depending on the conductivity contrast, this contribution, $\varDelta A_{MW}$, can be very large, but its relaxation frequency, f_{MW} is low, of the order of magnitude of the charge relaxation frequency of the conductive medium. Finally, the third relaxation mechanism, the Maxwel-Wagner-O'Konski (MWO) one, is due to the polarization of the counter-ion cloud around a charged colloidal particle [14, 16, 24, 25]. This contribution, $\varDelta A_{MWO}$, is particularly large for aqueous systems due to the large dissociating power of water and the resulting large surface charge of the particles. However, we expect it to be less relevant to our case, due to the use of the apolar solvent dodecane. We note, nevertheless, that the MWO relaxation frequency, f_{MWO}, can be significantly larger than both f_{MW} and f_{ch} [15, 30, 43]. In our specific experimental conditions, with the field applied using external electrodes, the sensitivity of the experiment to the field-induced order is strongly dependent on the relaxation frequency of the different mechanisms responsible for the particle reorientation. Indeed, at low frequencies, $f < f_{ch}$, the field inside the sample is screened by the double-layer of conductive charges built-up on the capillary wall in front of the electrodes. This process has exactly the same physical origin and approximately the same relaxation frequency as the MW effect. Therefore, for $f < f_{ch}$, where the MW contribution, $\varDelta A_{MW}$, is large, the field applied to the particle is strongly attenuated and the electro-optic signal is weak. We note that, in a similar way, the contributions of other low-frequency electro-kinetic processes, like the α-relaxation [17], can be neglected in our case.

The experimental results for $\varDelta A(f)$ are presented in Fig 10. The part of the curve below $f_{max} = 500$ Hz is not suitable for comparison with the models because in this region the internal field, acting on the particles, differs from the applied field due to the relaxation of the solvent conductivity charges, centered around $f_{ch} = 20$ Hz. However, above f_{max}, the screening of the applied field is negligible and this "high-frequency" region can be used for the comparison with the theory. Qualitatively, only one relaxation process is observed, with characteristic frequency of a few kHz, followed by a high-frequency plateau, which can be identified with $\varDelta A_{diel}$. Therefore, the relaxing part of $\varDelta A$ should be due to MW or/and MWO mechanism.
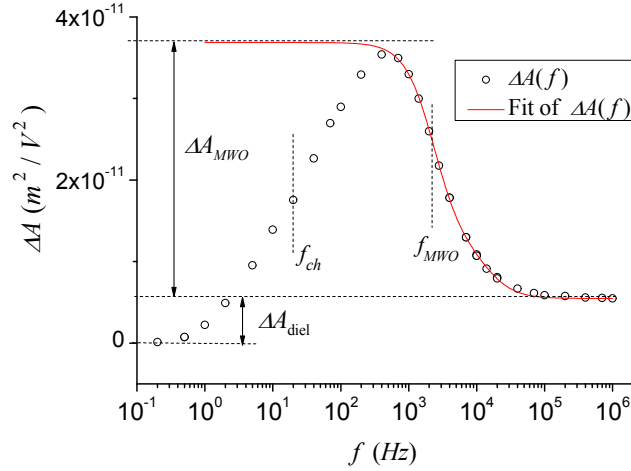
Fig 10: Frequency dependence of the coupling coefficient ΔA. The fit (red line) is limited to the region $f \geq 500\ Hz$ $>> f_{ch}$ in which the field is not screened by the mobile charges in the solvent.

However, the relaxation frequency is two orders of magnitude higher than f_{ch}. This is incompatible with a MW relaxation process which should give a contribution much closer to f_{ch}. This confirms, quite unexpectedly, that the large contribution at $f \approx f_{max}$ is due to the MWO process, despite the apolar character of the solvent. The best fit of our data with the dielectric and MWO theoretical formulae is shown in Fig. 10, giving $\Delta A_{diel} = 5.7 \times 10^{-12}\ m^2/V^2$, $\Delta A_{MWO} = 2.4 \times 10^{-11}\ m^2/V^2$ and $f_{MWO} = 2300\ Hz$. This ΔA_{diel} value is rather high for the moderate aspect ratio of the nanorods, which indicates that the dielectric constant of the pigment is $\varepsilon_p \approx 10.6$. This value is higher than for most organic solids but it is comparable to that of camphor and some of its derivatives, as well as to those of some other solids [44]. Using this value and the fit result for f_{MWO}, we obtain $\kappa_\sigma = 7 \times 10^{-14}\ S$ for the equivalent surface conductivity of the particles. Assuming that the mobility of the charges in the counter-ion cloud around the particles is of the usual order of magnitude, $\mu_\sigma \approx 10^{-8}\ m^2/(V.s)$, we estimate the surface charge density of the particles, $q_\sigma = \kappa_\sigma/\mu_\sigma \approx 7 \times 10^{-6}\ C/m^2$. As expected, the surface charge of the particles is very small, about 4 orders of magnitude smaller than the usual values reported in aqueous colloidal dispersions. However, the equivalent contribution to the bulk conductivity of the particle, due to the polarization of the counter-ion cloud, is $\kappa_{eq} \approx 4\kappa_\sigma / L$ [30], where $L \approx 100\ nm$ is the average size of the particle. We obtain then $\kappa_{eq} \approx 3 \times 10^{-6}\ S/m$, i.e. the equivalent conductivity of the nanorod is orders of magnitude larger than the bulk conductivity of the solvent, $\kappa_s = 2.2 \times 10^{-9}\ S/m$. Therefore, due to the high efficiency of the MWO mechanism, the pigment particles respond to the field as metal nanorods immersed in a perfect insulator, a situation much similar to that observed in aqueous colloidal systems such as dispersions of beidellite nanosheets or imogolite nanotubes [11, 30]. To test the validity of these estimated values, we use them to recalculate the MWO contribution to the coupling coefficient, obtaining $\Delta A_{MWO} = 4.3 \times 10^{-11}\ m^2/V^2$, which is about twice larger than the experimental value from Fig. 10. Taking into account the

number of approximations used in the numerical calculations (considering the particles as monodisperse spheroids with high aspect ratio), the agreement is quite good and the MWO mechanism does explain satisfactorily the experimental results.

3.2. Field-induced dichroism in the sandwich-cell geometry

The study of the field-induced orientational order is also possible using thin flat cells which are very well-suited for the optic and electro-optic investigations of liquid crystals (Fig. 2(b)). This cell geometry is particularly interesting from the point of view of the potential electro-optic applications of colloidal dispersions. Indeed, large cells of this kind are easy to produce and very strong fields can be applied to thin cells (with a cell gap d of the order of ten microns) using low voltages. However, a serious drawback of this geometry is that the field is applied along the cell normal, i. e. along the usual direction of light propagation. Therefore, the transient birefringence, $\Delta n(E)$, is very hard to measure because the optic response is isotropic and only the ordinary index $n_o(E)$ is probed, making the study of the field-induced order $S(E)$ much more difficult and less sensitive.

To avoid this difficulty inherent to the flat-cell geometry, we investigated the field-induced order by measuring the variation of the cell absorbance under field. The component $a_\perp(E)$ is the only one experimentally accessible. However, taking into account that $a_{iso} = const. = a_\perp(0)$, we obtain from Eq. (1) $R(E) = 1 - a_\perp(E)/a_\perp(0)$ and $R^{sat} = 1 - a_\perp(E = \infty)/a_\perp(0)$. Finally, this gives

$$S(E) = \frac{a_\perp(0) - a_\perp(E)}{a_\perp(0) - a_\perp(E = \infty)} = \frac{\log I(E) - \log I(0)}{\log I(E = \infty) - \log I(0)}, \tag{3}$$

where $I(E)$ is the measured transmitted light intensity (either polarized or unpolarized since it corresponds to $I_\perp(E)$ in both cases.)

The transient signals of the cell transmittance under field pulses (E = 2.05 $V/\mu m$) at different frequencies are presented in Fig. 11(a). When the field is applied, the particles align with their long axis parallel to **E** and the transmission increases, confirming that $a_\perp < a_\parallel$, i.e. that the absorption dipole moment is on average along the rod axis. The effect of the field is larger at lower frequency. Qualitatively, this shows that the coupling of the particle with the field decreases with increasing frequency. Fig 11(b) presents the cell transmittance as a function of the field amplitude for $f = 100\ kHz$. As expected, the transmittance increases with increasing field and almost saturates at $E = 5\ V/\mu m$. Under strong fields, the transmittance rapidly reaches a maximum and then relaxes slightly (and slowly), which indicates a small decrease of the induced order, probably due to the Joule heating of the suspension.
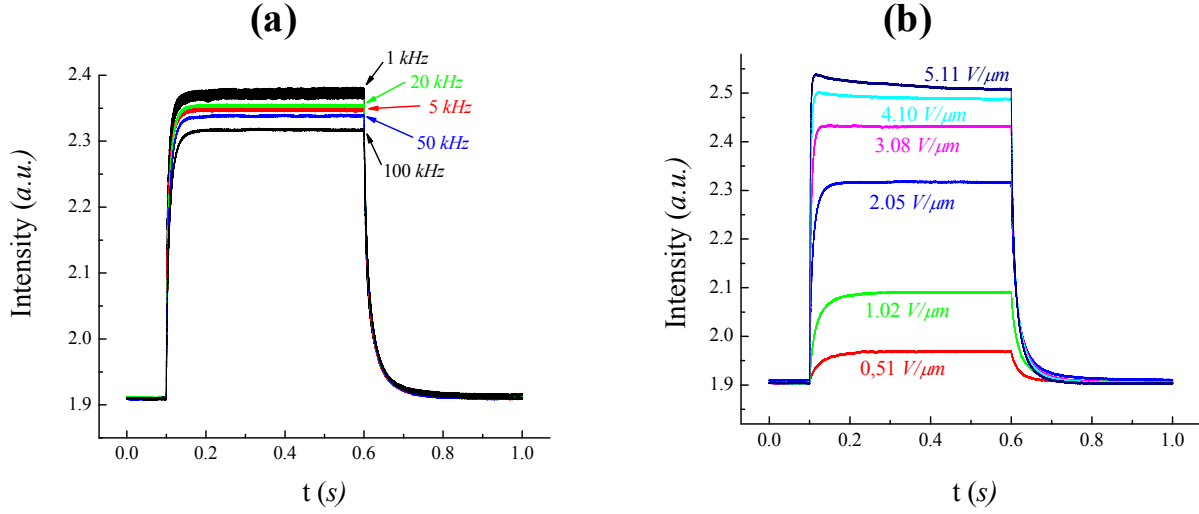
Fig. 11: Transient transmittance signal of the cell under 500 ms long burst of a square waveform (a) at fixed field amplitude ($E = 2.05$ $V/\mu m$) and different frequencies; (b) at fixed field frequency ($f = 100$ kHz) and different amplitudes.

By plotting the field-dependence of the transmitted intensity, I (E) versus E^2, and extrapolating the curve to $E = \infty$, we obtain the saturated value of the intensity, $I(E = \infty)$. Substituting it in Eq. (3), we derive the field-dependence of the order parameter for $f = 100$ kHz (see Fig. 12(a)). From the initial slope of that curve, we obtain the saturating field, $E^{sat} = 1.60$ $V/\mu m$, in excellent agreement with the value 1.66 $V/\mu m$ obtained with the capillary sample. Such good agreement confirms the validity of our approach which consists in only measuring $I_{\perp}(E)$ to infer the order parameter. Such agreement also confirms that the suspension in the flat cell is not altered by any significant contamination due to the seal and the large area of the glass surfaces. Finally, it also confirms that, at this high frequency, the field penetration inside the suspension is quite the same in the two drastically different experimental geometries.

The transmitted intensity $I(E)$ depends on the field frequency. However, its saturated value, $I(E \to \infty)$ is frequency independent because it corresponds to completely oriented pigment particles with order parameter $S(E \to \infty) = 1$. Therefore, we can use the value of $I(E \to \infty)$ obtained at 100 kHz for the analysis of the $I(E)$ data measured at any frequency. The $S(E)$ results obtained in this way are shown in Fig. 12(b). At high frequencies, $f \geq 20$ kHz, the $S(E)$ curves are almost superposed: the order parameter increases monotonously with the field and saturates to the theoretically expected $S = 1$ value. At lower frequencies, however, the behavior of $S(E)$ changes: it saturates to a value $S < 1$ and even decreases significantly with increasing field for $f < 10$ kHz. This is most probably due to the mass flow induced by the electric field, to Joule heating of the suspension, to electrohydrodynamic instabilities in the induced nematic phase, and to charge injection from the ITO electrodes.

We note that the saturation of the order parameter to $S = 1$ at high frequency indicates that these artifacts are avoided or at least significantly minimized above $f = 20\ kHz$.

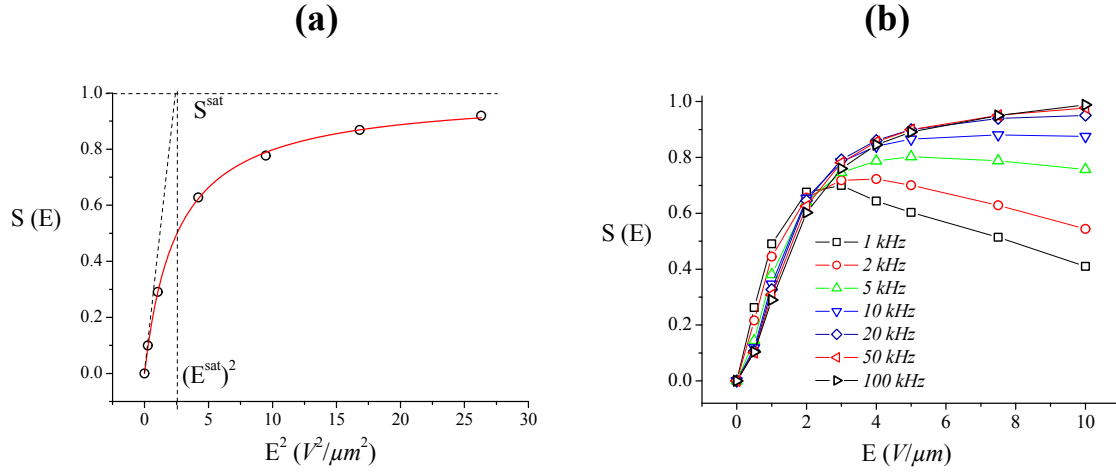**(a)**   **(b)**

Fig. 12: Electric-field-induced order parameter in the isotropic suspension of pigment particles: (a) Field-dependence of the order parameter for $f = 100\ kHz$. The open symbols are the experimental results, the red solid line is the hyperbolic extrapolation curve and the dashed lines show how the E^{sat} value is obtained; (b) Variation of the field-induced order parameter with the frequency of the applied waveform.

At low field, $E < 1\ V/\mu m$, the $S(E)$ curves increase monotonously for the whole explored range of frequencies, showing that the above-mentioned artifacts are negligible. From the initial slope of the S / E^2 curves, we obtain the frequency dependence of the saturating field E^{sat} (Fig. 13) and we compare it with the values obtained by the birefringence measurements in capillary samples. Qualitatively, the two sets of results show a similar behavior, with E^{sat} increasing with the frequency and saturating to approximately 1.6 $V/\mu m$. However, at low frequency, the E^{sat} results from the flat cell are somewhat higher than those measured with the capillary. This difference is easy to understand when taking into account that the flat cell data are measured with a square waveform. Indeed, for a given frequency f, the response of the sample to the square waveform is an average over all the (odd) harmonics of f. As the higher frequencies correspond to higher E^{sat} values (see in Fig. 13 the curve measured with a sinusoidal waveform), the average E^{sat} value for the square waveform is higher. Hence, once again, we obtain a good agreement of the results from the two different experimental techniques and sample geometries.
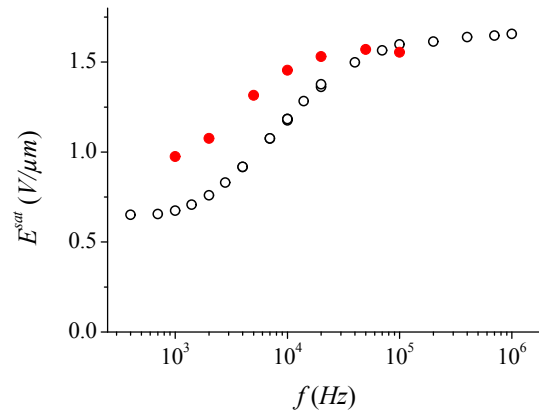
Fig. 13: Frequency dependence of the saturating field E^{sat} measured by dichroism in the flat cell (full red symbols: square waveform) and by transient birefringence in a capillary (open symbols: sinusoidal waveform).

3.3. SAXS measurement of the electric-field-induced orientational order

SAXS measurements were performed by applying the electric field in-situ to the colloidal dispersions of pigment nanorods to confirm the field-induced particle alignment. One advantage of this technique, compared to optical ones, is that it provides direct information on the orientation of the nanorods, at the microscopic level. Typical SAXS patterns, measured in a capillary cell with and without field, are presented in Fig. 14. As expected, the pattern is completely isotropic ($S = 0$) in zero-field. Under increasing a.c. sinusoidal field (at $f = 2$ kHz), the SAXS patterns become more and more anisotropic because of the induced nematic-like orientational order ($S > 0$). This anisotropy can be related to S by applying well-documented procedures [45, 46] involving numerical simulations of the patterns.
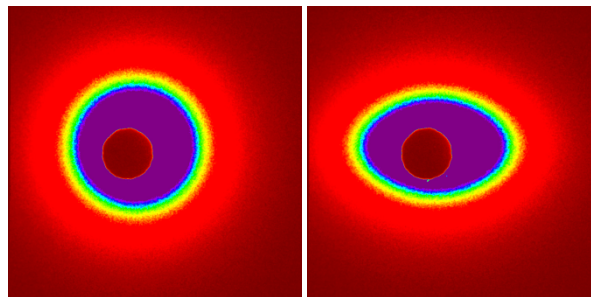

Fig. 14: SAXS images taken in absence of electric field (left) and with applied field $E = 960$ V/mm (right).
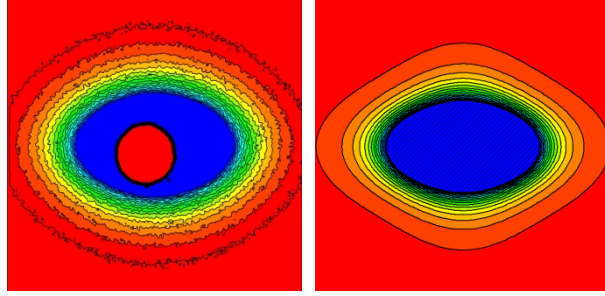
Fig. 15: Contour plots of the experimental SAXS pattern recorded with applied field $E = 960$ V/mm (left) and the numerical simulation with polydisperse particles and induced order parameter $S = 0.46$ (right).

These simulations rely on the following assumptions: The particles are considered as polydisperse cylinders with log-normal distribution laws for L and D. The average values of the two distributions, $L_{av} = 250$ nm and $D_{av} = 50$ nm, and the standard deviations, $\sigma_L = 50$ nm and $\sigma_D = 20$ nm, were derived from the TEM images, see section 2.1 above. The orientational distribution function of the particles under field is supposed to be Maier-Saupe-like [47, 48]. For each particle the coupling parameter ΔA is calculated as a function of its volume and aspect ratio L/D under the assumption that the alignment is due to the MWO mechanism and the particles are perfect cylinders with high aspect ratio, $L/D \gg 1$. Naturally, for the isotropic case ($S = 0$), the contour lines of the simulated SAXS intensity are circles. Upon increasing order parameter ($S > 0$), the contour lines become anisotropic, and their axial ratio, R_{cl}, increases monotonously with S, as expected. However, the shape of the simulated contour lines is not exactly the same as that of the experimental ones. This discrepancy is probably due to the rough approximation of the particles as perfect cylinders with high aspect ratio. Moreover, for both experimental patterns and numerical simulations, the anisotropy of the contour lines increases slowly with decreasing scattering vector q_s. Nevertheless, to find the field-induced order parameter we compare the simulated contour axial ratio R_{cl} with the experimental one. The best agreement for $E = 960$ $V/\mu m$ is obtained with $S = 0.46$ $\pm$ 0.08 for a particle with the statistically average dimensions, L_{av} and D_{av}. This value is in good agreement with the values obtained from the two dichroic measurements at this field, $S = 0.50$ (recalculated for $f = 2$ kHz from Fig. 9) and $S = 0.44$ (experimental value from Fig. 12). This agreement shows that the field-induced orientational order revealed at the macroscopic scale by optical techniques fairly reflects that prevailing at the nanoparticle scale.

4. Conclusions

We investigated the electric-field-induced order in an isotropic colloidal suspension of Pigment Red 176 nanorods in dodecane. Three different experimental techniques were applied, namely transient birefringence, transient dichroism and SAXS. Two different kinds of sample cells were used: flat optical capillaries with the

field applied along the capillary axis by external electrodes, and flat sandwich cells with the field applied parallel to the sample normal by internal ITO electrodes. The order parameter, birefringence and dichroism induced by short d.c. pulses or by bursts of a.c. field were investigated in a large frequency range, 0.2 Hz to 1 MHz, and for fields up to E_{rms} = 5 $V/\mu m$ for which the induced order reaches its theoretically maximal value of S = 1. The detailed birefringence study showed that the contribution of the permanent dipole moment **μ** of the nanorods to the induced order is negligible. On the contrary, the contribution of the excess polarizability **α** of the particles is large, indicating that, despite the apolar organic solvent and the low surface charges of the particles, the main alignment mechanism is MWO, i.e. the polarization of the counter-ion cloud surrounding the charged particle. The dichroic and SAXS investigations, complementary to the transient birefringence, confirm this conclusion.

The high efficiency of the electric field to align the particles, with field-induced order parameter saturating to S = 1 under moderate fields, and the response times of a few milliseconds, make the isotropic dispersions of Pigment Red 176 nanorods in dodecane a promising system for electro-optical applications.

References

[1] A. de la Cotte, P. Merzeau, J.W. Kim, K. Lahlil, J.-P. Boilot, T. Gacoin, E. Grelet, Electric field induced birefringence in nonaqueous dispersions of mineral nanorods, Soft Matter, 11 (2015) 6595-6603.

[2] J.K.G. Dhont, K. Kang, Electric-field-induced polarization and interactions of uncharged colloids in salt solutions, Eur. Phys. J. E, 33 (2010) 51-68.

[3] J.K.G. Dhont, K. Kang, An electric-field induced dynamical state in dispersions of charged colloidal rods, Soft Matter, 10 (2014) 1987-2007.

[4] B. Frka-Petesic, B. Jean, L. Heux, First experimental evidence of a giant permanent electric-dipole moment in cellulose nanocrystals, EPL, 107 (2014).

[5] A.B. Golovin, O.D. Lavrentovich, Electrically reconfigurable optical metamaterial based on colloidal dispersion of metal nanorods in dielectric fluid, Appl. Phys. Lett., 95 (2009).

[6] J.S. Kamal, R. Gomes, Z. Hens, M. Karvar, K. Neyts, S. Compernolle, F. Vanhaecke, Direct determination of absorption anisotropy in colloidal quantum rods, Phys. Rev. B, 85 (2012) 035126.

[7] A. Kuijk, T. Troppenz, L. Filion, A. Imhof, R. van Roij, M. Dijkstra, A. van Blaaderen, Effect of external electric fields on the phase behavior of colloidal silica rods, Soft Matter, 10 (2014) 6249-6255.

[8] L.S. Li, A.P. Alivisatos, Origin and scaling of the permanent dipole moment in CdSe nanorods, Phys. Rev. Lett., 90 (2003) 097402.

[9] M. Mohammadimasoudi, Z. Hens, K. Neyts, Full alignment of dispersed colloidal nanorods by alternating electric fields, RSC Advances, 6 (2016) 55736-55744.

[10] T.J. Robb-Smith, K.J. Donovan, K. Scott, M. Somerton, Induced electro-optic effects in single-walled carbon nanotubes. I. Polarizability of metallic nanotubes, Phys. Rev. B, 83 (2011) 155414.

[11] E. Paineau, M.-E.M. Krapf, M.-S. Amara, N.V. Matskova, I. Dozov, S. Rouziere, A. Thill, P. Launois, P. Davidson, A liquid-crystalline hexagonal columnar phase in highly-dilute suspensions of imogolite nanotubes, Nat. Commun., 7 (2016) 10271.

[12] M.Y. Boltoeva, I. Dozov, P. Davidson, K. Antonova, L. Cardoso, B. Alonso, E. Belamie, Electric-Field Alignment of Chitin Nanorod-Siloxane Oligomer Reactive Suspensions, Langmuir, 29 (2013) 8208-8212.

[13] A. Peterlin, H.A. Stuart, Z. Phys., 112 (1939) 129-147.

[14] C.T. O'Konski, A.J. Haltner, Characterization of the monomer and dimer of tobacco mosaic virus by transient electric birefringence, J. Am. Chem. Soc., 78 (1956) 3604-3610.

[15] M. Saito, H.P. Schwan, G. Schwarz, Response of nonspherical biological particles to alternating electric fields, Biophys. J., 6 (1966) 313.

[16] C.T. O'Konski, S. Krause, Electric properties of macromolecules 6: Theory of Kerr constant of rigid conducting dipolar macromolecules, J. Phys. Chem., 74 (1970) 3243.

[17] P. Arenas-Guerrero, G.R. Iglesias, A.V. Delgado, M.L. Jimenez, Electric birefringence spectroscopy of montmorillonite particles, Soft Matter, 12 (2016) 4923-4931.

[18] F.J. Arroyo, A.V. Delgado, F. Carrique, M.L. Jimenez, T. Bellini, F. Mantegazza, Effect of ionic mobility on the enhanced dielectric and electro-optic susceptibility of suspensions: Theory and experiments, J. Chem. Phys., 116 (2002) 10973-10980.

[19] M.L. Jimenez, L. Fornasari, F. Mantegazza, M.C.D. Mourad, T. Bellini, Electric Birefringence of Dispersions of Platelets, Langmuir, 28 (2012) 251-258.

[20] W.L. Bragg, A.B. Pippard, The form birefringence of macromolecules, Acta Crystallogr., 6 (1953) 865-867.

[21] G. Schwarz, General equation for mean electrical energy of a dielectric body in an alternating electrical field, J. Chem. Phys., 39 (1963) 2387-2388.

[22] K.W. Wagner, Arch. Elektrotechnik, 2 (1914) 371.

[23] J.C. Maxwell, A treatise on electricity and magnetism, Unabridged 3d ed., Dover Publications, New York, 1954.

[24] C.T. O'Konski, Effect of interfacial conductivity on dielectric properties, J. Chem. Phys., 23 (1955) 1559-1559.

[25] C.T. O'Konski, Electric properties of macromolecules 5: Theory of ionic polarization in polyelectrolytes, J. Phys. Chem., 64 (1960) 605-619.

[26] A. Eremin, R. Stannarius, S. Klein, J. Heuer, R.M. Richardson, Switching of Electrically Responsive, Light-Sensitive Colloidal Suspensions of Anisotropic Pigment Particles, Adv. Funct. Mater., 21 (2011) 556-564.

[27] S. Kredentser, A. Eremin, P. Davidson, V. Reshetnyak, R. Stannarius, Y. Reznikov, Dynamic and permanent gratings in suspensions of absorbing nanocrystals in an organic solvent, Photonics Letters of Poland, 7 (2015) 91-93.

[28] R.J. Greasty, R.M. Richardson, S. Klein, D. Cherns, M.R. Thomas, C. Pizzey, N. Terrill, C. Rochas, Electro-induced orientational ordering of anisotropic pigment nanoparticles, Philos. Trans. Royal Soc. A, 371 (2013) 20120257.

[29] K. May, R. Stannarius, S. Klein, A. Erermin, Electric-Field-Induced Phase Separation and Homogenization Dynamics in Colloidal Suspensions of Dichroic Rod-Shaped Pigment Particles, Langmuir, 30 (2014) 7070-7076.

[30] I. Dozov, E. Paineau, P. Davidson, K. Antonova, C. Baravian, I. Bihannic, L.J. Michot, Electric-Field-Induced Perfect Anti-Nematic Order in Isotropic Aqueous Suspensions of a Natural Beidellite Clay, J. Phys. Chem. B, 115 (2011) 7751-7765.

[31] Y. Kurioz, Y. Reznikov, O. Tereshchenko, I. Gerus, O. Buluy, K.R. Ha, D.H. Kim, S.B. Kwon, S.K. Park, Highly sensitive photoaligning materials on a base of cellulose-cinnamates, Mol. Cryst. Liq. Cryst., 480 (2008) 81-90.

[32] P. van Vaerenbergh, J. Léonardon, M. Sztucki, P. Boesecke, J. Gorini, L. Claustre, F. Sever, J. Morse, T. Narayanan, An upgrade beamline for combined wide, small and ultra small-angle x-ray scattering at the ESRF, AIP Conf. Proc., 1741 (2016) 030034.

[33] E. Paineau, I. Dozov, A.-M. Philippe, I. Bihannic, F. Meneau, C. Baravian, L.J. Michot, P. Davidson, In-situ SAXS Study of Aqueous Clay Suspensions Submitted to Alternating Current Electric Fields, J. Phys. Chem. B, 116 (2012) 13516-13524.

[34] G.B. Thurston, D.I. Bowling, Frequency dependence of Kerr effect for suspensions of rigid particles J. Colloid Interface Sci., 30 (1969) 34.

[35] I. Tinoco, K. Yamaoka, The reversing pulse technique in electric birefringence, J. Phys. Chem., 63 (1959) 423-427.

[36] F. Perrin, Mouvement Brownien d'un ellipsoide (II). Rotation libre et dépolarisation des fluorescences. Translation et diffusion de molécules ellipsoidales, J. Phys. Radium, 7 (1936) 1-11.

[37] F. Perrin, Mouvement brownien d'un ellipsoide - I. Dispersion diélectrique pour des molécules ellipsoidales, J. Phys. Radium, 5 (1934) 497-511.

[38] J.K. Park, J.C. Ryu, W.K. Kim, K.H. Kang, Effect of Electric Field on Electrical Conductivity of Dielectric Liquids Mixed with Polar Additives: DC Conductivity, J. Phys. Chem. B, 113 (2009) 12271-12276.

[39] Blinov L.M., ChigrinovV.G., Electrooptic Effects in Liquid Crystal Materials, Springer1994.

[40] O.P. Boiko, R.M. Vasyuta, V.G. Nazarenko, V.M. Pergamenshchik, Y.A. Nastishin, O.D. Lavrentovich, Polarizing properties of functional optical films based on lyotropic chromonic liquid crystals, Mol. Cryst. Liq. Cryst., 467 (2007) 181-194.

[41] B. Norden, A. Davidsson, Form dichroism and study of molecular shape, Chemical Physics, 30 (1978) 177-186.

[42] O. Wiener, Die Theorie des Mischkörpers für das Feld der stationären Stromung., Abh. sdchs. Ge8. (Akad.) Wiss., 32 (1912) 509-604.

[43] D.A. Saville, T. Bellini, V. Degiorgio, F. Mantegazza, An extended Maxwell-Wagner theory for the electric birefringence of charged colloids, J. Chem. Phys., 113 (2000) 6974-6983.

[44] S.O. Morgan, W.A. Yager, Dielectric Properties of Organic Components Relation to Chemical Composition and Physical Structure, Ind. Eng. Chem. Res., 32 (1940) 1519-1528.

[45] E. Helfer, P. Panine, M.F. Carlier, P. Davidson, The interplay between viscoelastic and thermodynamic properties determines the birefringence of F-actin gels, Biophys. J., 89 (2005) 543-553.

[46] J.B. Hayter, J. Penfold, Use of viscous shear alignment to study anisotropic micellar structure by small-angle neutron-scattering, J. Phys. Chem., 88 (1984) 4589-4593.

[47] W. Maier, A. Saupe, Eine einfache molekular-statistische Theorie der nematischen kristallinflüssigen Phase. 1., Z. Naturforsch. A, 14 (1959) 882-889.

[48] W. Maier, A. Saupe, Eine einfache molekular-statistische Theorie der nematischen kristallinflüssigen Phase. 2., Z. Naturforsch. A, 15 (1960) 287-292.